INTERPOLATED AND WARPED 2-D DIGITAL WAVEGUIDE MESH ALGORITHMS

Vesa Välimäki

Lab. of Acoustics and Audio Signal Processing
Helsinki University of Technology
vesa.valimaki@hut.fi

Lauri Savioja

Telecommun. Software and Multimedia Lab.
Helsinki University of Technology
lauri.savioja@hut.fi

ABSTRACT

Interpolated and warped digital waveguide mesh algorithms have been developed to overcome the problem caused by direction and frequency-dependence of wave travel speed in digital waveguide mesh simulations. This paper reviews the interpolation methods applicable in the two-dimensional case. The bilinear interpolation technique and two other approaches are briefly recapitulated. The use of 2-D quadratic interpolation results in a mesh structure that is efficiently implemented using only additions and binary shifts. The optimized interpolated 2-D mesh is obtained by choosing the free parameters of the interpolation method so that the difference in wave travel speed in the axial and diagonal directions is minimized. The output signal of any digital waveguide mesh can be processed with a warped FIR filter to reduce the dispersion error at all frequencies. The frequency-warping factor must be optimized individually for each mesh structure. We introduce an extended method called multiwarping, which can be used to further decrease the dispersion error. The frequency range of digital waveguide mesh simulations is also discussed.

1. INTRODUCTION

The digital waveguide mesh was introduced in 1993 by Van Duyne and Smith [1, 2]. They showed that the method is suitable for sound synthesis of percussion instruments although it suffers from direction-dependent dispersion. In 1994, Savioja *et al.* extended the use of the digital waveguide mesh to three dimensions, and presented simulation results of wave propagation in acoustic spaces [3]. The method has turned out to be useful in acoustic design of listening rooms, for example. Recently, the digital waveguide mesh has been used in the modeling of drums [4] and the violin body [5].

The interpolated mesh was developed to overcome the direction-dependent wave propagation characteristics and dispersion error [6]. However, it was only possible to reduce the direction-dependence while the dispersion was not much affected—it was merely rendered almost independent of direction. Luckily, the remaining dispersion error can be made considerably smaller using frequency warping [6–9]. It is implemented by postprocessing the output signal of the mesh using a warped FIR filter. Fontana and Rocchesso have also shown that the frequency-warping can be incorporated in the mesh structure [10]. The best results so far have been obtained by using the triangular waveguide mesh [11–13] together with a warped FIR filter [14, 6]. Also, the interpolated rectangular mesh can be improved considerably using frequency warping [6].

In Section 2 of this paper, we review the interpolation methods for the rectangular 2-D digital waveguide mesh. In Section 3 we discuss frequency-warping methods and introduce a novel approach, multiwarping. Section 4 focuses on the frequency range of digital waveguide simulations. It is suggested that the available frequency range can be extended with the interpolation and warping methods. In Section 5, it is shown by numerical examples how much the different mesh algorithms can gain from the interpolation and frequency-warping techniques, when the warping factor is optimized individually for each of them. Section 6 concludes the paper and presents directions for future work.

2. DIGITAL WAVEGUIDE MESH ALGORITHMS

2.1. Original Digital Waveguide Mesh

The 'original' digital waveguide mesh [1, 2] consists of a rectangular grid where the signal value at every node is updated at each sampling interval according to the following formula:

$$p_c(n) = \frac{1}{2}\sum_{k=1}^{4} p_k(n-1) - p_c(n-2) \tag{1}$$

where n is the discrete time index, $p_c(n)$ is the node to be updated, $p_k(n-1)$ are its four nearest neighbors, and $p_c(n-2)$ is the value of the center node two sample intervals ago. Thus, it is necessary to store two complete meshes.

The first part of the update step (1) can also be formulated using the following matrix (see also [6], Eq. (15))

$$h_{\text{orig}} = \frac{1}{2}\begin{bmatrix} 0 & 1 & 0 \\ 1 & 0 & 1 \\ 0 & 1 & 0 \end{bmatrix} \tag{2}$$

This interpretation is equivalent to the notion of point-spreading function used in image processing.

Figures 1(a) and 2(a) show two different views of the wave propagation speed in the original mesh as a function of two frequency variables. The wave travel speed is constant in diagonal directions, while in other directions the speed decreases with frequency, that is, the dispersion error increases. This is also seen in Fig. 2(b) that shows the minimal (diagonal) and maximal (axial) relative frequency error (RFE) caused by dispersion. For details on computing the RFE curves, see [6].

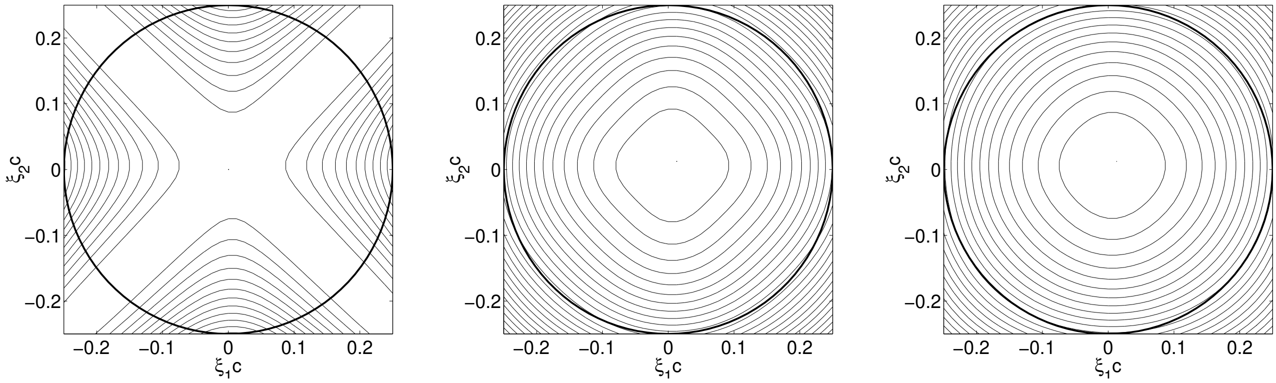

Figure 1. Equal wave travel speed contours for the (a) original, (b) bilinearly interpolated, and (c) optimally interpolated digital waveguide mesh where contours descend from the center point in increments of 1%. The distance from the center gives the normalized temporal frequency $f = c\xi$, and $\angle(\xi_1, \xi_2)$ determines the propagation direction. The circle (thick line) indicates the highest normalized temporal frequency of the rectangular waveguide mesh, which is 0.25.

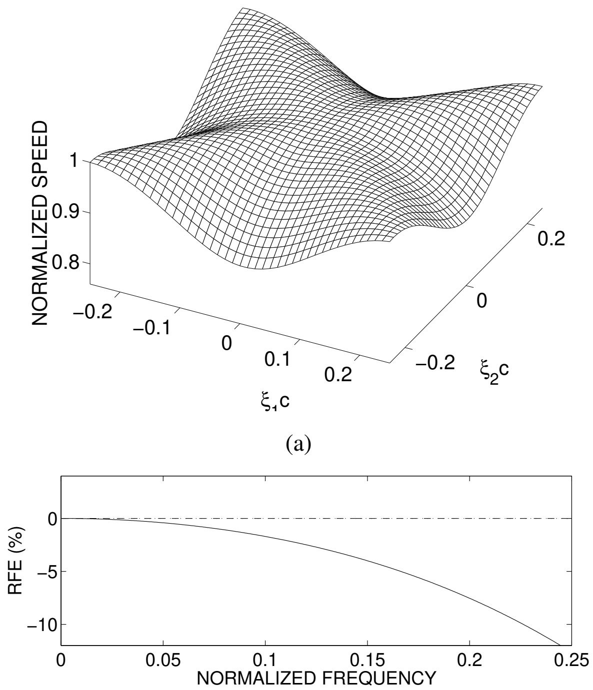

Figure 2. (a) Normalized wave travel speed in the original digital waveguide mesh as a function of two normalized frequency variables $c\xi_1$ and $c\xi_2$, and (b) the minimal (dashed line) and maximal (solid line) RFE.

2.2. Bilinearly Interpolated Waveguide Mesh

The aim of the interpolated waveguide mesh was to suppress the direction-dependence and dispersion of the original waveguide mesh [6]. The motivation was that sample updates should occur in more directions than just four as in the original mesh. The interpolation technique effectively inserts new nodes in the mesh—the contribution of the hypothetical nodes is then spread on the existing neighboring nodes to obtain a realizable structure. This is a 2-D application of fractional delay filters [15]. The method of superimposing signal samples onto a non-integer point of a digital delay line was introduced in [16], where this operation was named as 'deinterpolation'. See also [17, pp. 128–135], where deinterpolation is discussed in detail.

In the initial version of the interpolated mesh algorithm [6], four hypothetical nodes were inserted in diagonal directions, and we chose to use bilinear interpolation, which is a two-dimensional extension of linear interpolation. In this case, the point-spreading function is

$$h_{\text{bilin}} = \frac{1}{4}\begin{bmatrix} \frac{1}{2} & \sqrt{2} & \frac{1}{2} \\ \sqrt{2} & 6-4\sqrt{2} & \sqrt{2} \\ \frac{1}{2} & \sqrt{2} & \frac{1}{2} \end{bmatrix} = \begin{bmatrix} 0.1250 & 0.3536 & 0.1250 \\ 0.3536 & 0.08579 & 0.3536 \\ 0.1250 & 0.3536 & 0.1250 \end{bmatrix} \quad (3)$$

In the bilinearly interpolated mesh, the wave travel speed is not constant in any direction, but the behavior is more homogeneous as a function of direction than in the original mesh, as seen by comparing Figs. 1(a) and 1(b). The remaining dispersion causes the mode frequencies of the acoustic system that is being modeled to be lower than they should, as illustrated by the RFE curve in Fig. 3(a). Fortunately, the error is practically independent of direction, and hence a single correction function can be used to reduce the frequency error.

2.3. Quadratic 2-D Interpolation

It is also possible to use higher-order interpolation to implement the interpolated mesh. Here we present the use of second-order Lagrange interpolation, or quadratic interpolation, which leads to the following point-spreading function:

$$h_{\text{quad}} = \frac{1}{4}\begin{bmatrix} \frac{1}{4} & \frac{3}{2} & \frac{1}{4} \\ \frac{3}{2} & 1 & \frac{3}{2} \\ \frac{1}{4} & \frac{3}{2} & \frac{1}{4} \end{bmatrix} = \begin{bmatrix} 0.06250 & 0.3750 & 0.06250 \\ 0.3750 & 0.2500 & 0.3750 \\ 0.06250 & 0.3750 & 0.06250 \end{bmatrix} \quad (4)$$

Note that convolution with this kernel can be realized without multiplications, since all the elements in (4) are easily implemented as binary shifts and additions.

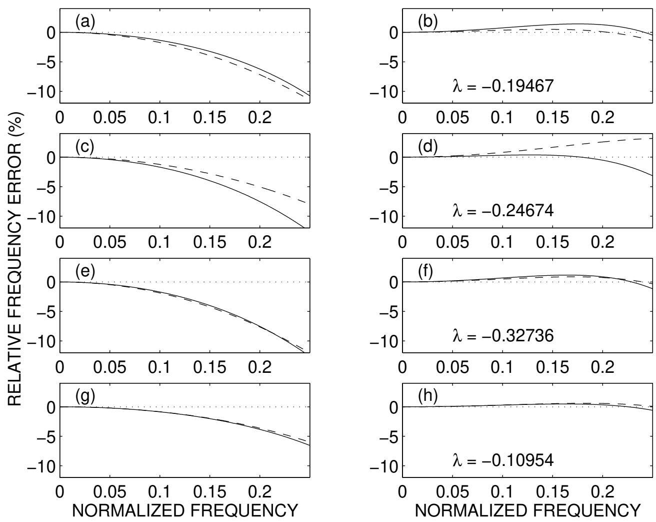

Figure 3. Maximal and minimal (dashed and solid lines) relative frequency error in the (a) bilinearly, (c) quadratically, and (e) optimally interpolated, and (g) the triangular mesh. The corresponding RFEs after frequency warping are displayed on the right. The dotted line indicates the zero error.

Figure 3(c) shows the RFE of the interpolated mesh when quadratic interpolation is used. Perhaps surprisingly, the quadratic interpolation does not yield as good results as the bilinear interpolation. The reason is that the quadratic interpolation has to work outside its optimal range, which is $-0.5 \le d \le 0.5$ in each direction, where d is the fractional delay from the node to be updated (see [17, pp. 90–94] for a discussion on approximation errors of Lagrange interpolation filters). The delay values required in this interpolation problem are $d = -0.7071$ and $d = 0.7071$.

Note that it is impossible to use higher-order polynomial interpolation with the 3-by-3 point-spreading function. For example, the use of third-order Lagrange interpolation would lead to a 5-by-5 matrix.

2.4. Optimized 2-D Interpolation

There are only three free parameters in the 3-by-3 point-spreading functions: the diagonal, axial, and central value. It is thus relatively easy to optimize the values of these coefficients so that the best possible characteristics are achieved. We have optimized the coefficients of the 3-by-3 matrix so that the difference between the minimal and maximal frequency error below the normalized frequency 0.25 is minimized while the error at the zero frequency is forced to zero [6]. The iteration yields the following point-spreading function:

$$h_{\text{opt}} = \begin{bmatrix} 0.09398 & 0.3120 & 0.09398 \\ 0.3120 & 0.3759 & 0.3120 \\ 0.09398 & 0.3120 & 0.09398 \end{bmatrix} \qquad (5)$$

The resulting wave travel speed is shown in Fig. 1(c), and the corresponding RFE curves in axial and diagonal directions are in Fig. 3(e). It can be seen that the difference between the two extreme cases of RFE curves is smaller than for the other interpolated rectangular meshes.

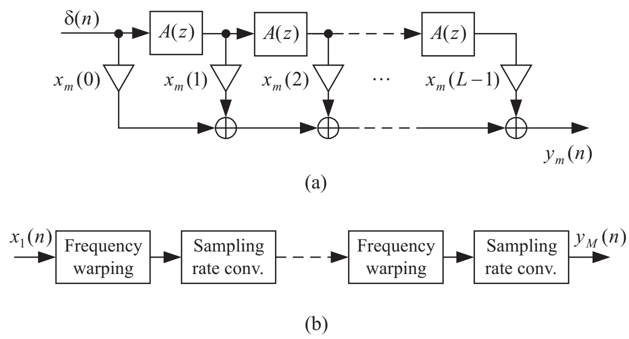

Figure 4. (a) Frequency warping can be implemented using a chain of identical first-order allpass filters. (b) Multiwarping is realized by alternating first-order frequency-warping operations and sample rate conversions.

2.5. Triangular Digital Waveguide Mesh

Also other sampling lattices than the rectangular one have been considered for digital waveguide mesh models. The triangular mesh has been found to be a good choice [11–13]. Figure 3(g) indicates that the RFE in the triangular mesh is smaller than in any of the rectangular mesh structures discussed above. In addition, the difference between the smallest and largest error is small. The main drawback of the triangular mesh is the triangular tessellation of the plane, which may be more complicated than the rectangular one in some cases.

3. FREQUENCY-WARPING TECHNIQUES

The dispersion error appearing in digital waveguide mesh simulations can be reduced using frequency warping, when the error is almost identical in all directions and the error function is monotonic and relatively smooth [14, 6]. Then it is possible to design a frequency-warping filter, which shifts the frequencies and reduces the error when the output signal of the digital waveguide mesh $x(n)$ is processed with it.

3.1. How to Use Frequency Warping

Frequency warping can be implemented with a warped FIR filter, which consists of a chain of first-order allpass filters $A(z)$, as shown in Fig. 4(a) [7, 6, 9]. The tap coefficients are set equal to the signal samples $x_m(n)$ to be warped, i.e., the output signal of the digital waveguide mesh in this case. When a unit impulse is fed into the filter, the warped signal $y_m(n)$ is obtained at the output. The extent of warping is controlled by the allpass filter coefficient λ that we call the warping factor. In addition, a sampling rate conversion is required, because all frequencies—not only the high frequencies—are shifted as a consequence of frequency warping (see [6] for details).

3.2. Reduction of Dispersion Error

We have optimized λ for each case so that the maximal RFE in the frequency band from 0 up to 25% of the sampling rate is minimized. Figure 3(b) presents the RFE of the bilinearly interpolated mesh after its output signal has been frequency warped using warping factor $\lambda = -0.19467$. Note that the RFE has been considerably reduced at high frequencies, enabling accurate wideband simulations. Figure 3(d) corresponds to the warped quadratically interpolated mesh, which is not so successful because the difference between the minimal and maximal error curves gets large at middle and high frequencies.

The RFE of the warped optimally interpolated mesh shown in Fig. 3(f) is superior over other interpolated rectangular mesh algorithms. Its maximum RFE is 1.2%. However, the warped triangular mesh [14, 6] produces the smallest RFE (0.6%) of all possibilities, see Fig. 3(h).

3.3. Multiwarping

For some time, our aim has been to find a new frequency-warping method to augment the degrees of freedom. It would be desirable to have a technique in which the accuracy could be enhanced at will by selecting a higher order warping operation. Formerly, such a technique has not been available. In theory, it would be possible to use higher order allpass transfer functions $A(z)$ instead of the first-order one. However, replacing unit delays with second or higher order allpass filters leads to both folding and warping in the delay-line implementation [18], which is undesirable. Another attractive solution would be to apply the first-order warping many times successively, but this is a waste of effort since there will not be more degrees of freedom in this procedure than in a single frequency warping. This can be shown by noting that the frequency warping obtained with two successive warping operations with λ_1 and λ_2 is equivalent to warping with $(\lambda_1 + \lambda_2) / (1 + \lambda_1\lambda_2)$.

We propose a new approach that we call 'multiwarping' [19], where an arbitrary number of successive first-order frequency warping and resampling operations are performed alternately as illustrated in Fig. 4(b). The use of sampling rate conversions facilitates the design of nonlinear frequency shifts that are impossible to achieve with a single warping, since at a new sampling rate, the frequency shifts occur at different frequencies. The sampling rate conversions are done by factor D, such that if $0 < D < 1$ the process is upsampling (interpolation) and if $D > 1$ it is downsampling (decimation).

There are various strategies to find the optimal values for the warping and resampling coefficients. It is a multivariable optimization task, which should be restricted so that the downsampling operations do not cut the effective frequency band too much. Another criterion to take into account is that if λ is close to 1.0 the output signal of frequency warping becomes long, since the pole of the allpass filter is located close to the unit circle.

4. EXTENDING THE FREQUENCY RANGE

In this section, we discuss the question of the upper frequency limit of the interpolated and warped waveguide mesh simulations. It is known that the limiting frequency in the case of the original waveguide mesh is 0.25, and above that frequency only mirror images of lower frequencies occur [1]. However, when interpolation and frequency-warping methods are used, it is no longer obvious what the highest frequency is. In the following, we demonstrate how it is possible to extend the frequency range of digital waveguide mesh simulations. Fontana and Rocchesso have discussed earlier that the triangular mesh is superior over rectangular or hexagonal tilings in terms of valid frequency band [20].

Figure 5 shows the mapping of the original normalized frequencies to the frequencies occurring on the mesh in the case of the original (Fig. 5(a)) and optimally interpolated meshes, when

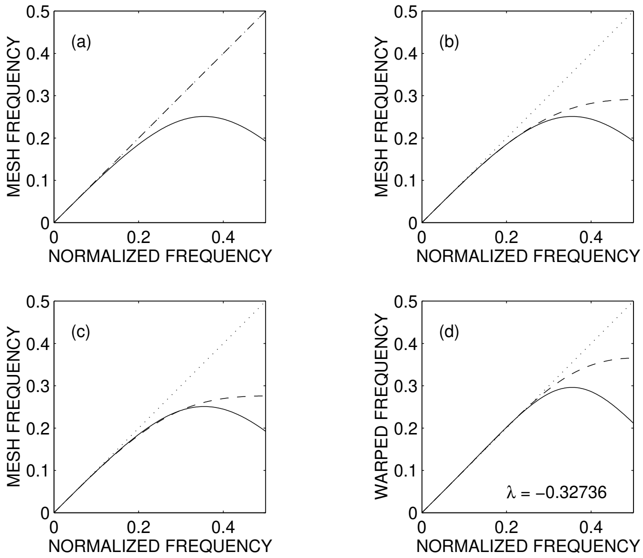

Figure 5. Mapping of frequencies in the (a) original, (b) optimally interpolated (up to 0.25), and (c) another optimally interpolated (up to 0.35) waveguide mesh (d) together with warped mapping for case b. The axial direction is shown with the solid and the diagonal direction with the dashed line. The dotted line indicates the desired ideal mapping function (y = x).

the frequency limit has been set to 0.25 (in Fig. 5(b)) and 0.35 (in Fig 5(c)). The maximum value of all axial mapping curves is 0.2500, and it occurs at normalized frequency 0.3536. This appears to be the highest frequency that can be simulated using the rectangular digital waveguide meshes. Frequency warping could at its best shift the mesh frequencies so that 0.3536 would again occur at the right frequency. Assuming ideal frequency warping, the remaining error is caused by the differences between different directions.

As an example, we display in Fig. 5(d) the frequency mapping of the warped interpolated mesh optimized up to the normalized frequency 0.25. The warping factor used is $\lambda = -0.32736$. It can be seen that both the axial and diagonal frequency mappings follow the ideal mapping curve (dotted line in Fig. 5(d)) well until about 0.25. Above this frequency, also the difference between the diagonal and axial properties of the mesh begins to increase substantially, and it is impossible to extend the bandwidth much higher. However, it would be possible to warp the interpolated mesh that has been optimized up to 0.35 (see Fig. 5(c)), and then it would be feasible to obtain a good accuracy up to 0.35.

5. NUMERICAL EXAMPLES

In the following we present numerical examples to illustrate the properties of the methods discussed above. We have simulated a square membrane with rigid boundaries (reflection coefficient –1) using different digital waveguide mesh algorithms, and compared the results. The mesh size was 16 × 16 nodes. For details of the simulation, see [6]. Figure 6 shows the magnitude spectra of the simulated membrane in three cases: (a) the original, (b) the warped optimized interpolated, and (c) the warped triangular digital waveguide mesh. The ideal magnitude spectrum is given for comparison in each case.

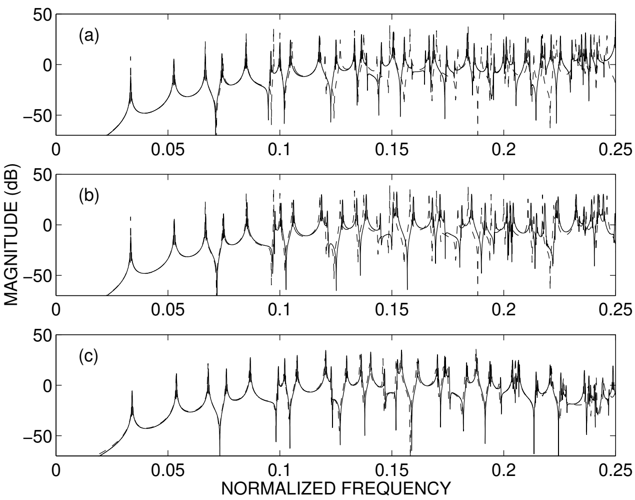

Figure 6. Magnitude spectrum of an ideal rectangular membrane (dashed lines) together with the simulation results (solid lines) obtained with the (a) original, (b) the warped optimally interpolated, and (c) the warped triangular mesh.

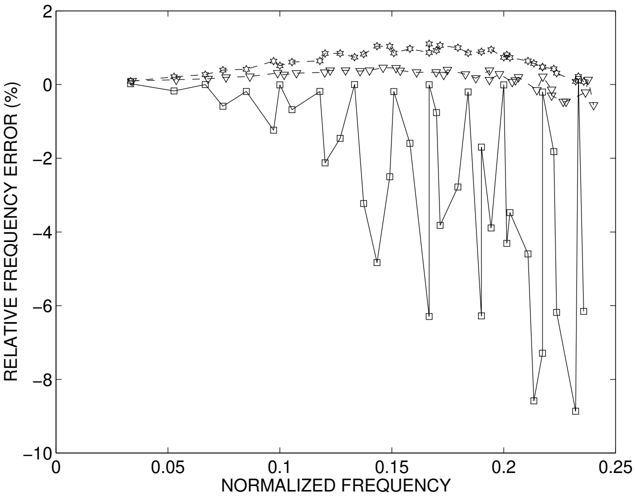

Figure 7. Error in eigenmode frequencies of the simulated rectangular membrane (squares = original mesh, hexagrams = warped interpolated mesh, triangles = warped triangular mesh).

The errors in the frequencies of eigenmodes of the membrane, as a difference from the ideal eigenfrequencies calculated by the Rayleigh equation, are given in Fig. 7. The error behavior of the original mesh reveals that some eigenmodes occur at nearly the correct frequency while others are too low by several percent. This is explained by the non-homogeneous nature of the original mesh (see Figs. 1(a) and 2(a)).

The errors in the warped interpolated mesh are smaller—they are within ±1.2% in the frequency band from 0 to 25% of the sampling rate (see Fig. 7). However, the warped triangular mesh is still better: the maximum error on the same frequency band is only 0.60%. These results are in good agreement with the theoretical RFE curves presented in Figs. 3(f) and 3(h), since the mode frequency errors are found between the theoretical minimum and

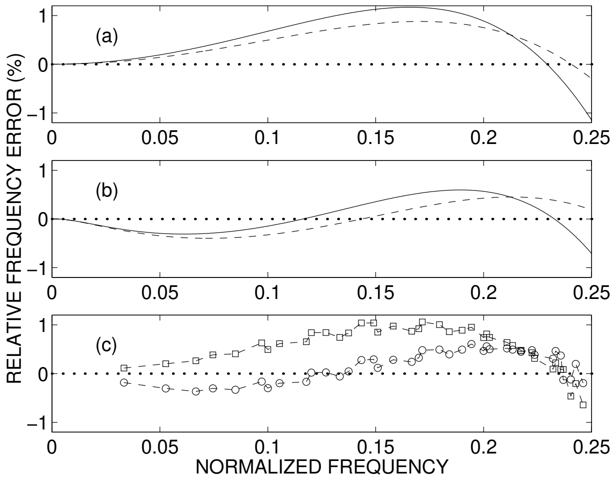

Figure 8. RFE in the optimally interpolated (a) warped and (b) multiwarped waveguide mesh with (c) a comparison of the corresponding eigenmode frequency errors obtained from a numerical simulation of a membrane (squares = warped, circles = multiwarped).

maximum errors in all cases. It must be understood that if the RFE is positive, the mode frequencies given by a simulation are shifted up, and if the RFE is negative, the frequencies are shifted downwards.

To reduce the error further, multiwarping consisting of a chain of two frequency-warping and resampling operations can be performed, as illustrated in Fig. 4(b). Finding the optimal warping and resampling factors is not trivial. In the case of performing both warping and sampling rate conversion twice, there are four variables. Of these only three are free, since the last resampling must be performed such that there will be no shifts at the lowest frequencies. In this case, we applied the Fmins function in Matlab to search for the optimal values for the two warping factors and one resampling coefficient. The resulting values $\lambda_1 = 0.919225$, $D_1 = 0.998377$, $\lambda_2 = -0.988548$, and $D_2 = 7.32022$ give the maximal RFE of 0.62% for the optimally interpolated rectangular mesh, which is about one half of the error obtained with a single warping (1.2%). The corresponding RFE curves are presented in Fig. 8(a) and 8(b).

Figure 8(c) represents the RFE obtained by simulating the square membrane with the warped and multiwarped interpolated digital waveguide meshes. The line with squares in Fig. 8(c) stands for the result with one frequency warping and is in good agreement with the curves shown in Fig. 8(a). The curve with circles in Fig. 8(c) corresponds to the multiwarped case shown in Fig. 8(b). This example demonstrates that the error in mode frequencies can be halved using multiwarping.

Similar results have been obtained with the triangular digital waveguide mesh, where the error can be reduced from 0.60% to 0.35% by using a two-stage multiwarping instead of one warping.

Adding more frequency-warping and resampling operations to the multiwarping can further reduce the error. The difference between the maximal and minimal error, i.e., the direction-dependence, will restrict the improvement that can be achieved using multiwarping. As the number of cascaded warping and resampling operations is increased, the computational load increases almost linearly. Since multiwarping must be executed as an off-line method, such as postprocessing after a simulation run in our application, the increase in computation time is not very critical.

6. CONCLUSIONS AND FUTURE WORK

This paper reviewed various interpolated and warped digital waveguide mesh algorithms and discussed the frequency range of digital waveguide mesh simulations. The rectangular mesh using quadratic interpolation can be implemented without multiplications. The optimized interpolated mesh is better than other interpolated rectangular mesh structures having a 3-by-3 matrix as the point-spreading function. The warped triangular mesh produces simulation results with the smallest dispersion error.

The multiwarping technique was also discussed. The method consists of successive frequency-warping and resampling operations. The maximal RFE of the interpolated or triangular digital waveguide mesh is reduced by about 50% by using two cascaded frequency-warping procedures and sampling rate conversions instead of a single warping and resampling.

6.1. Directions for Future Research

Digital waveguide mesh methods are still not well understood. There are many issues related to wave propagation that cannot be implemented accurately yet. These include modeling of internal losses of the medium and reflections at the boundaries. In the case of wall reflections, it would be necessary to be able to model the acoustical properties of materials as a function of frequency but also as a function of incident angle. A straightforward implementation of a reflection that consists of inserting a filter behind the wall, next to the last layer of nodes, yields a direction-dependent behavior, which only works as planned for a plane wave arriving along the diagonal axis of a rectangular mesh.

While this paper concentrated on the two-dimensional digital waveguide mesh methods, the interpolation and frequency-warping methods are applicable to three-dimensional simulations as well. Promising results have been published in [21], where the interpolation technique was adapted to the 3-D rectangular digital waveguide mesh.

7. ACKNOWLEDGMENTS

The work of V. Välimäki has been supported by a postdoctoral research grant from the Academy of Finland.

8. REFERENCES

[1] S. Van Duyne and J. O. Smith, “Physical modeling with the 2-D digital waveguide mesh,” in *Proc. Int. Computer Music Conf.*, Tokyo, Japan, pp. 40–47, Sept. 10–15, 1993.

[2] S. Van Duyne and J. O. Smith, “The 2-D digital waveguide mesh,” in *Proc. IEEE WASPAA*, New Paltz, NY, Oct. 1993.

[3] L. Savioja, T. Rinne, and T. Takala, “Simulation of room acoustics with a 3-D finite difference mesh,” in *Proc. Int. Computer Music Conf.*, Aarhus, Denmark, pp. 463–466, Sept. 1994.

[4] M. Aird, J. Laird, and J. Fitch, “Modelling a drum by interfacing 2-D and 3-D waveguide meshes,” in *Proc. Int. Computer Music Conf.*, Berlin, Germany, pp. 82–85, Aug. 2000.

[5] P. Huang, S. Serafin, and J. O. Smith, “A waveguide mesh model of high-frequency violin body resonances,” in *Proc. Int. Computer Music Conf.*, Berlin, Germany, pp. 86–89, Aug. 2000.

[6] L. Savioja and V. Välimäki, “Reducing the dispersion error in the digital waveguide mesh using interpolation and frequency-warping techniques,” *IEEE Trans. Speech and Audio Processing*, vol. 8, no. 2, pp. 184–194, Mar. 2000.

[7] A. Oppenheim, D. Johnson, and K. Steiglitz, “Computation of spectra with unequal resolution using the fast Fourier transform,” *Proc. IEEE*, vol. 59, pp. 299–301, Feb. 1971.

[8] M. Karjalainen, A. Härmä, U. K. Laine, and J. Huopaniemi, “Warped filters and their audio applications,” in *Proc. IEEE WASPAA*, New Paltz, NY, Oct. 1997.

[9] A. Härmä, M. Karjalainen, L. Savioja, V. Välimäki, U. K. Laine, and J. Huopaniemi, “Frequency-warped signal processing for audio applications,” *J. Audio Eng. Soc.*, vol. 48, 2000. In press.

[10] F. Fontana and D. Rocchesso, “Online correction of dispersion error in 2D waveguide meshes,” in *Proc. Int. Computer Music Conf.*, Berlin, Germany, pp. 78–81, Aug. 2000.

[11] F. Fontana and D. Rocchesso, “A new formulation of the 2D waveguide mesh for percussion instruments,” in *Proc. Colloquio di Informatica Musicale*, Bologna, Italy, pp. 27–30, Nov. 1995.

[12] S. Van Duyne and J. O. Smith, “The 3D tetrahedral digital waveguide mesh with musical applications,” in *Proc. Int. Computer Music Conf.*, Hong Kong, pp. 9–16, Aug. 1996.

[13] F. Fontana and D. Rocchesso, “Physical modeling of membranes for percussion instruments,” *Acustica united with Acta Acustica*, vol. 84, no. 3, pp. 529–542, May/June 1998.

[14] L. Savioja and V. Välimäki, “Reduction of the dispersion error in the triangular digital waveguide mesh using frequency warping,” *IEEE Signal Processing Letters*, vol. 6, no. 3, pp. 58–60, Mar. 1999.

[15] T. I. Laakso, V. Välimäki, M. Karjalainen, and U. K. Laine, “Splitting the unit delay—Tools for fractional delay filter design,” *IEEE Signal Processing Mag.*, vol. 13, no. 1, pp. 30–60, Jan. 1996.

[16] V. Välimäki, M. Karjalainen, and T. I. Laakso, “Fractional delay digital filters,” in *Proc. IEEE Int. Symp. on Circuits and Systems*, Chicago, IL, vol. 1, pp. 355–358, May 1993.

[17] V. Välimäki, *Discrete-Time Modeling of Acoustic Tubes Using Fractional Delay Filters*. Doctoral thesis. Helsinki Univ. of Tech., Lab. of Acoustics and Audio Signal Process., Espoo, Finland, Dec. 1995. Available online at the following URL: `http://www.acoustics.hut.fi/publications/`.

[18] J. A. Moorer, “The manifold joys of conformal mapping: applications to digital filtering in the studio,” *J. Audio Eng. Soc.*, vol. 31, no. 11, pp. 826–841, Nov. 1983.

[19] L. Savioja and V. Välimäki, “Multiwarping for enhancing the frequency accuracy of digital waveguide mesh simulations,” unpublished manuscript, submitted for publication, 2000.

[20] F. Fontana and D. Rocchesso, “Signal-theoretic characterization of waveguide mesh geometries for membrane simulation,” in *Proc. Int. Computer Music Conf.*, Ann Arbor, MI, pp. 260–263, Oct. 1998.

[21] L. Savioja, “Improving the three-dimensional digital wave–guide mesh by interpolation,” in *Proc. Nordic Acoustical Meeting*, Stockholm, Sweden, pp. 265–268, Sept. 1998.